Biomaterials 74 (2016) 245–255

Contents lists available at ScienceDirect

Biomaterials

journal homepage: www.elsevier.com/locate/biomaterials

Improvement of diaphragmatic performance through orthotopic application of decellularized extracellular matrix patch

M. Piccoli [a, *, 1], L. Urbani [b, ***, 1], M.E. Alvarez-Fallas [a], C. Franzin [a], A. Dedja [c], E. Bertin [a], G. Zuccolotto [d], A. Rosato [e, f], P. Pavan [g, h], N. Elvassore [i], P. De Coppi [b, ****], M. Pozzobon [a, **]

[a] Stem Cells and Regenerative Medicine Lab, Fondazione Istituto di Ricerca Pediatrica Città della Speranza, Padua, Italy
[b] Stem Cells & Regenerative Medicine Section, Developmental Biology & Cancer Programme, UCL Institute of Child Health and Great Ormond Street Hospital, London, United Kingdom
[c] Department of Cardiac, Thoracic and Vascular Sciences, University of Padua, Padua, Italy
[d] Department of Medicine, University of Padua, Padua, Italy
[e] Veneto Institute of Oncology IOV – IRCCS, Padua, Italy
[f] Department of Surgery, Oncology and Gastroenterology, University of Padua, Padua, Italy
[g] Department of Industrial Engineering, University of Padua, Padua, Italy
[h] Centre for Mechanics of Biological Materials, University of Padua, Padua, Italy
[i] Department of Industrial Engineering, University of Padua, and Venetian Institute of Molecular Medicine, Padua, Italy

ARTICLE INFO

Article history:
Received 3 June 2015
Received in revised form
29 September 2015
Accepted 1 October 2015
Available online 9 October 2015

Keywords:
Extracellular matrix
Decellularization
Skeletal muscle
Regenerative medicine

ABSTRACT

Muscle tissue engineering can provide support to large congenital skeletal muscle defects using scaffolds able to allow cell migration, proliferation and differentiation. Acellular extracellular matrix (ECM) scaffold can generate a positive inflammatory response through the activation of anti-inflammatory T-cell populations and M2 polarized macrophages that together lead to a local pro-regenerative environment. This immunoregulatory effect is maintained when acellular matrices are transplanted in a xenogeneic setting, but it remains unclear whether it can be therapeutic in a model of muscle diseases. We demonstrated here for the first time that orthotopic transplantation of a decellularized diaphragmatic muscle from wild animals promoted tissue functional recovery in an established atrophic mouse model. In particular, ECM supported a local immunoresponse activating a pro-regenerative environment and stimulating host muscle progenitor cell activation and migration. These results indicate that acellular scaffolds may represent a suitable regenerative medicine option for improving performance of diseased muscles.

1. Introduction

In the last few years, extracellular matrix (ECM) scaffolds derived from decellularized tissues have been successfully used to repair a variety of damaged or diseased organs, such as heart [1–3], skin [4], oesophagus [5,6] and trachea [7,8]. Application in skeletal muscle field has also been investigated [9], but the engineering of a functional muscle tissue has only been partially explored [10–17]. Up to now, regeneration or reconstruction of skeletal muscle tissue with cell therapy has not been completely successful [18], in particular using aged animal models where the ECM is already fibrotic or damaged [19,20]. Moreover, cellular engraftment in muscles such as the diaphragm, it is limited. In this work, we explored the possibility of implanting a decellularized muscle to determine *in vivo* response, potential therapeutic improvement and

* Corresponding author. Stem Cells and Regenerative Medicine Lab, Istituto di Ricerca Pediatrica Città della Speranza, Corso Stati Uniti 4, 35127 Padova, Italy.
** Corresponding author. Stem Cells and Regenerative Medicine Lab, Istituto di Ricerca Pediatrica Città della Speranza, Corso Stati Uniti 4, 35127 Padova, Italy.
*** Corresponding author. Stem Cells & Regenerative Medicine Section, Developmental Biology& Cancer Programme, UCL Institute of Child Health, 30 Guilford Street, London WC1N 1EH, United Kingdom.
**** Corresponding author. Stem Cells & Regenerative Medicine Section, Developmental Biology& Cancer Programme, UCL Institute of Child Health, 30 Guilford Street, London WC1N 1EH, United Kingdom.
E-mail addresses: m.piccoli@irpcds.org (M. Piccoli), l.urbani@ucl.ac.uk (L. Urbani), Paolo.DeCoppi@gosh.nhs.uk (P. De Coppi), m.pozzobon@irpcds.org (M. Pozzobon).
[1] These authors equally contributed to the work.

http://dx.doi.org/10.1016/j.biomaterials.2015.10.005

application of this biomaterial in complex tissue engineering approaches. Using decellularized scaffolds in tissue engineering can provide a valid method for the treatment of skeletal muscle damage and diseases, based on the fact that a biological scaffold possesses the great advantage to closely resemble the native tissue [21]. Skeletal muscle ECM plays an important role in tissue maintenance and regeneration, modulating cell adhesion and migration, growth factor storage and release, and stem cell homeostasis, activation and differentiation [22,23]. It remains partially unclear which cellular types contribute to the remodelling, however it is well established that macrophages play a major role for skeletal muscle regeneration and turn over [24,25]. Macrophages are activated in response to tissue damage or infection, causing an increase in the production of cytokines, chemokines and other inflammatory molecules to which they are exposed. Their remarkable plasticity leads to exhibit distinct and frequently opposite phenotypes when in contact with different environmental stimuli. Several works showed that the major effect of ECM application in skeletal muscle, both with same or different origin of recipient tissue, is to stimulate anti-inflammatory macrophages, leading to a constructive-type remodelling response [26,27]. Moreover, using a xenotransplantation model, we recently demonstrated that the implanted scaffold can modulate the immune response inhibiting rejection through an increased level of inhibitory cytokines and decreased levels of pro-inflammatory molecules. This mechanism of action is probably mediated by the presence of M2 monocytes that drive the response directly or through interaction with T-cell subset [28]. In addition, ECM degradation products yield by action of macrophages, positively influence proliferation and differentiation of muscle precursor cells and myoblasts responsible for the regenerative maintenance of skeletal muscle tissue [9,29]. However, it remains to determine whether ECM could promote remodelling and improve functional outcome on a diseased skeletal muscle.

With the aim of investigating promotion of repair of damaged/diseased skeletal muscle by a biological-derived scaffold, we generated and deeply characterized a decellularized diaphragmatic tissue. We proved that maintaining original composition and stiffness, ECM-derived scaffolds were able to activate immune regulated pathways when transplanted *in vivo*. This process led to a local pro-regenerative environment through activation of resident precursor cells, both in healthy and diseased mouse model.

2. Results

2.1. Generation and characterization of diaphragmatic decellularized matrix

Diaphragm muscles from wild type (wt) mice were treated with the detergent-enzymatic treatment (DET) protocol. We firstly investigated the number of cycles appropriate to obtain a complete cell removal using from 1 to 4 DET cycles. After each cycle, treated tissues appeared clearer and DNA amount significantly decreased, without differences between third and fourth cycle (Fig. 1A, B. Fresh: 225.5 ± 91.2; c1: 87.5 ± 26.1; c2: 21 ± 7.1; c3: 12.5 ± 3.5; c4: 8 ± 0.2 ng/μL). This result was confirmed also by nuclei counting after staining with DAPI (Fig. 1C, D. Fresh: 135.6 ± 24.6; c1: 83.6 ± 10.5; c2: 57 ± 20.8; c3: 5.9 ± 5; c4: 2.3 ± 3 nuclei/area), emphasizing that 3 DET cycles were necessary but enough to achieve more than 95% of nuclei depletion.

In parallel, we analysed ECM preservation after each DET cycle. The overall thickness of the diaphragmatic muscle after decellularization remained comparable to the fresh counterpart, suggesting no significant difference in matrix 3D architecture after treatment (Fig. 1E, F). Histological analyses revealed that the structure and the most important ECM components, such as collagen, sGAG and elastin, were preserved after 3 cycles (Fig. 1G–I). Maintenance of major components was confirmed also by protein quantification, which showed that only sGAG concentration decreased significantly after 3 cycles (Fig. 1G. Fresh: 0.57 ± 0.05; c3: 0.30 ± 0.13 μg/mg wet tissue).

Scanning electron microscopy (SEM) analysis of the acellular diaphragmatic matrix showed preservation of the micro- and ultra-architecture of the tissue, with maintenance of the 3D arrangement and conservation of myofibre structure and ECM (Fig. 1J). Higher magnification electron microscopy images confirmed elimination of nuclei and visualized integrity of collagen fibres between the myofibres after the decellularization process. Moreover, conservation of main components and architecture of the matrix allowed to maintain mechanical properties similar to those of the fresh tissue, as showed by measuring membrane stiffness and elastic modulus of the acellular matrix (Fig. 1K, L). No statistical difference was evident in the membrane force versus strain analyses before (fresh) and after 3 cycles of decellularization. Importantly, elastic modulus of wt diaphragm before and after decellularization displayed no statistical significant changes (Fig. 1M).

2.2. In vivo implantation of the acellular matrix in wt mice

After analysing the acellular diaphragmatic muscle characteristics, we assessed the biological effects implanting *in vivo* wt ECM-derived scaffolds (patch) over a wild non-injured mouse diaphragm (Fig. 2A). Transplanted mice were analysed 4, 7, 15, 30 and 90 days after patch implantation (n = 4 mice each time point, and n = 4 mice as untreated control, 0 days). At sacrifice, the scaffold was still identifiable from the surrounding native diaphragm after 4, 7 and 15 days from implantation, whereas for the latest time points, the area of graft was marked only by the non-absorbable sutures used for surgery (Fig. 2B). At the moment of harvesting the tissues, variable levels of liver adhesion to the implanted patch were observed in all time points (Fig. 2C), as previously described in literature [30]. The presence or absence of liver adhesion did not affect the results obtained from further analyses and did not introduce other types of variability. Haematoxylin & Eosin (H-E) and Masson's Trichrome stains unveiled that both native diaphragm and patch were greatly remodelled during the treatment (Fig. 2D, F). The native tissue was stimulated to grow and the thickness significantly increased between 4 and 15 days post implantation (Fig. 2E). This modification was transient since thickness of the native tissue returned to basal physiological levels after 30 days post-implantation (Fig. 2D–F). On the contrary, the applied matrix was gradually invaded by resident cells and constantly remodelled. Patch thickness started decreasing significantly after only 7 days, while 90 days later was almost completely reabsorbed (Fig. 2D, F, G). Cell migration into the originally acellular patch was evident from early time points. Native tissue cell activation was confirmed by Ki67 analysis: soon after patch implantation, resident cells began proliferating and migrating toward the acellular matrix (Fig. 2H), and this process reverted to physiological state 30 days after treatment (Fig. 2I).

2.3. Myogenic progenitor cell activation

Although the thickening of the native diaphragm after implanting the ECM-derived scaffold was proved, no significant difference in fibre cross sectional area (CSA) was found (Fig. 3A, B). Muscle growth seemed to derive from the generation of new fibres, as revealed by the presence of embryonic myosin heavy chain (Myh3) positive fibres in the native diaphragm, located in the region close to the patch in the earliest time points (Fig. 3E, F),

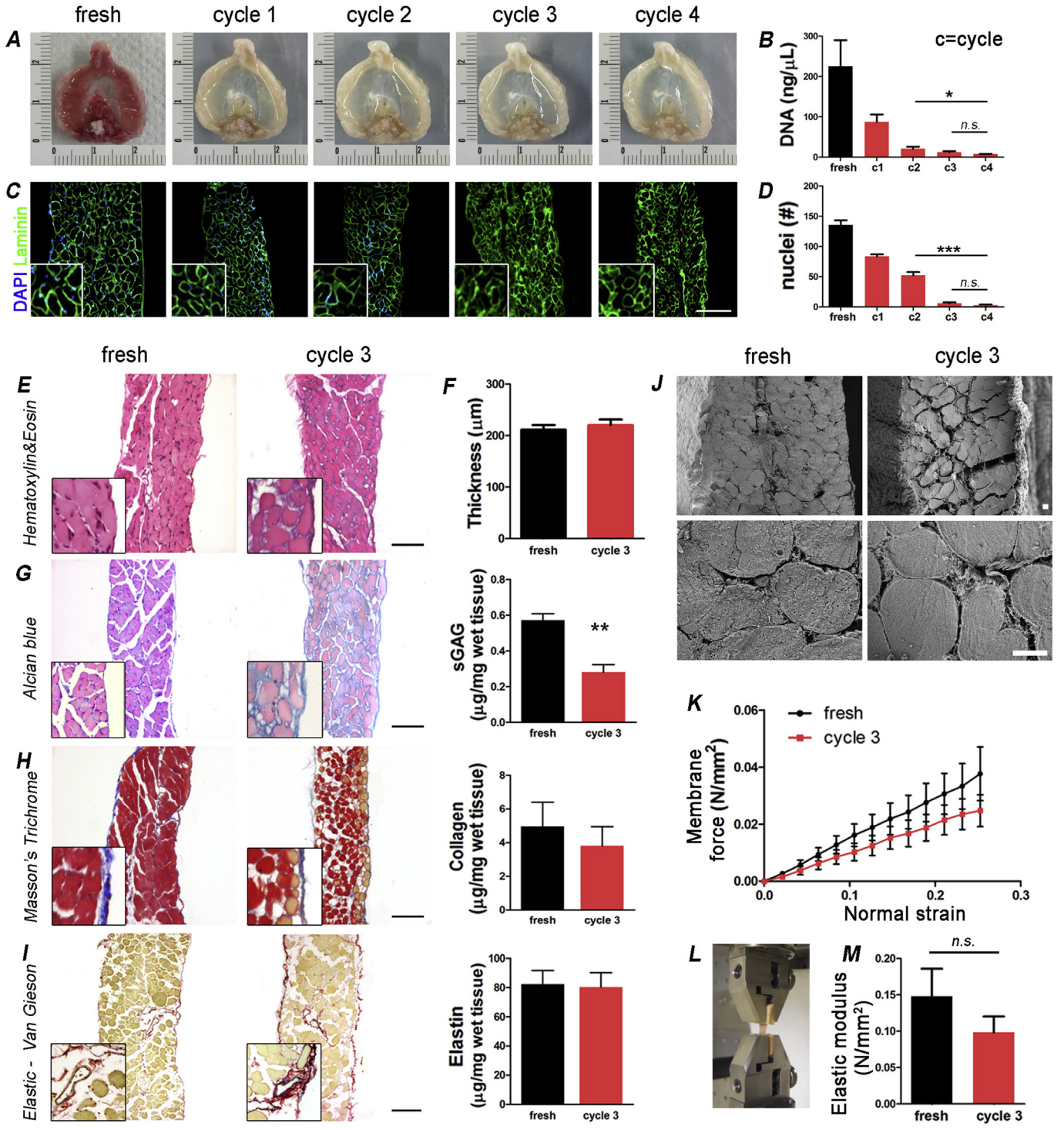

Fig. 1. Characterization of the diaphragmatic acellular scaffold. (A) Macroscopic appearance of wt diaphragmatic muscle after harvesting (fresh) and after each DET cycle; (B) DNA quantification (c = cycle); (C) Immunofluorescence of fresh and decellularized tissue after each DET cycle (n = 3) to discriminate remaining nuclei (DAPI) from tissue structure (Laminin); (D) Nuclei quantification analysing 5 random pictures per tissue sample (n = 3). (E) H–E staining on fresh and 3 DET cycle scaffold; (F) Fresh and decellularized tissue thickness; (G–I) Immunohistochemistry performed on fresh and 3 DET cycle scaffold to identify and quantify ECM proteins: Masson's Trichrome for collagen, Alcian blue for sGAG and Elastic-Van Gieson for elastin. Histograms are referred to the correspondent protein quantification; (J) SEM performed on fresh and decellularized scaffold after 3 DET cycles; (K–M) Stiffness and elastic modulus. *p < .05; **p < .01; ***p < .001; n.s. = not significant by Student *t*-test. Scale bar = 100 μm.

emphasizing the triggering effect of applied acellular matrix. Generation of new fibres was confirmed by the high *Myh3* gene expression rate in treated diaphragms in the earlier time points when compared to physiological levels (Supplementary Fig. 1). Furthermore, regenerating centre nucleated fibres were clearly present in the native tissue throughout all the time points (Fig. 3A). Generation of new muscle fibres and cellular colonization of patch were also supported by presence of activated myogenic precursor cells. From 7 to 30 days after patch implantation, Myf5 positive muscle precursor cells were located in the acellular matrix,

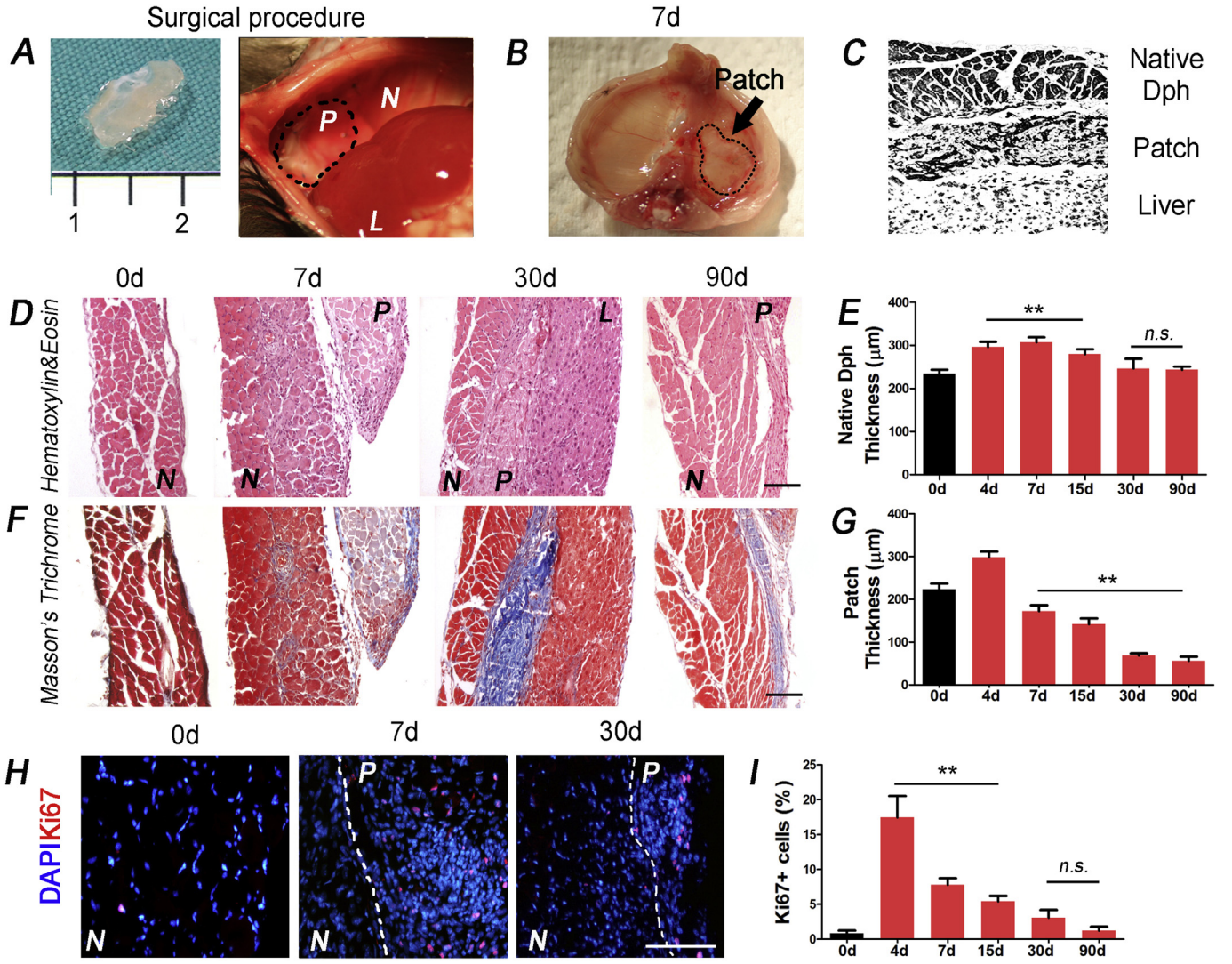

Fig. 2. *In vivo* scaffold implantation and local response. (A) Surgical procedure: decellularized matrix was sutured on the ventral side of diaphragm muscle of wt mice; (B) Macroscopic aspect of the treated diaphragm at day 7 after patch implantation; (C) Schematic representation of tissue arrangement *in vivo* after patch implantation (Dph = diaphragm); (D,F) Histological appearance of treated diaphragms after 0, 7, 30 and 90 days from implantation; (E,G) Thickness of native diaphragm and implanted patch throughout all the time points; (H–I) Immunofluorescence and quantification of proliferating Ki67 + cells. N = native tissue, P = patch, L = liver. **p < .01; n.s. = not significant by ANOVA and Student *t*-test. Scale bar = 100 μm.

highlighting a massive activation and migration of satellite cells from the recipient diaphragm into the acellular scaffold (Fig. 3C, D). The activation of this myogenic population was also supported by gene expression analysis in implanted muscles that revealed, at first, a strong induction of myogenic transcription factors such as *Myf5* and *Myogenin* between 4 and 15 days after treatment, and, secondly, a successive decrease toward physiological levels in parallel with the switching off of the regenerating process (Supplementary Fig. 1).

2.4. Macrophage response polarization toward an M2 phenotype

In vivo implantation of decellularized scaffold was associated with a significant increased presence of CD3 and CD4 expressing cells, especially within the fraction of FoxP3 positive cells (Fig. 4A–C). In particular, CD3 and CD4 followed a timing-dependent trend, with a maximum of expression at 7 days post implantation. At the same time point, higher number of CD4+FoxP3+ cells was found. As for other cell types, also this positive immune response revealed a reversible behaviour, decreasing to comparable level as the untreated muscles at the end of the analysed period. In parallel, we observed a progressive gain of macrophage antigen expression (CD68 + cells; Fig. 4F) and, most importantly, of M2 polarized cells, as evident by Arginase I expression, both at protein and gene level (Fig. 4D–I). When compared with the expression of pro-inflammatory M1 macrophage specific markers such as CD86 and *Nos2*, we obtained a ratio in favour of M2 anti-inflammatory macrophage population (Fig. 4G, J), both at protein and gene expression level, confirming the general remodelling effect.

2.5. Implantation of wild ECM-derived scaffold into an atrophic diaphragm

To confirm the anti-inflammation and pro-regenerative effect of implanted decellularized ECM also in a diseased environment, we treated 3 month-old *HSA-Cre*, $Smn^{F7/F7}$ atrophic mice (n = 4 mice for each time point, and n = 4 mice for untreated control, 0 days) with

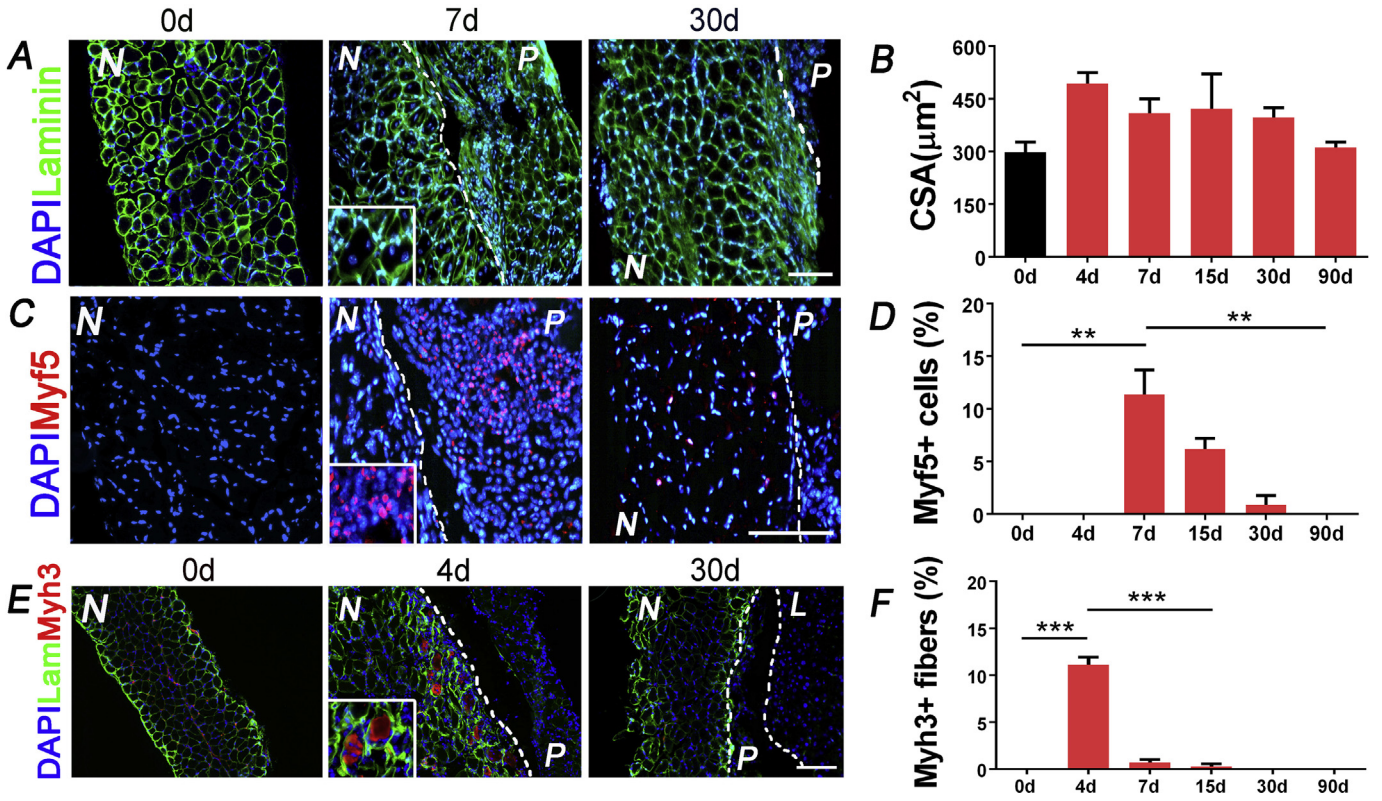

Fig. 3. Myogenic cell activation. (A) Immunostaining for Laminin of treated muscles at different time point; (B) Quantification of fiber cross sectional area (CSA) in sections at the analysed time points; (C–D) Immunostaining and quantification (% of cells) of Myf5+ precursor cells in treated samples; (E–F) Immunostaining and quantification of newly generated Myh3+ fibers. N = native tissue, P = patch, L = liver. **p < .01; ***p < .001 by ANOVA and Student *t*-test; scale bar = 100 μm.

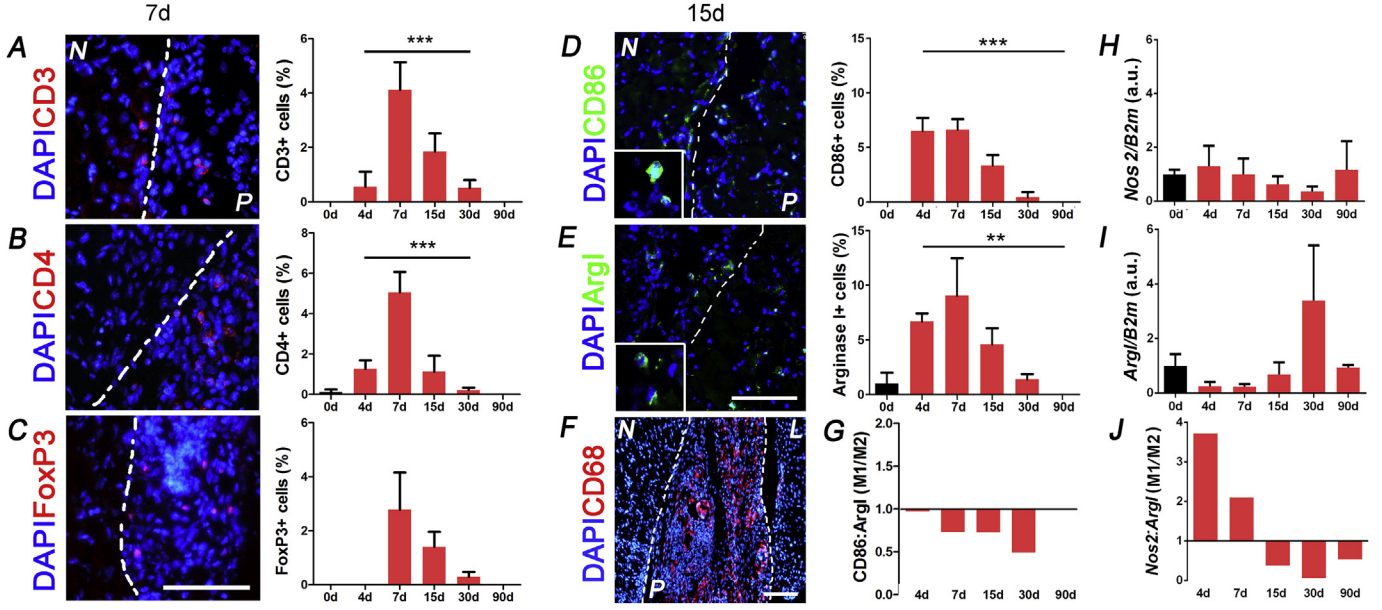

Fig. 4. Immunoreaction and macrophage polarization. (A–C) Representative immunofluorescence (7 days) and quantification of CD3+, CD4+ and FoxP3+ cells in the time course; (D–E) Immunofluorescence and quantification of CD86+ (M1 polarized) and Arginase I+ (M2 polarized) macrophages; (F) Immunofluorescence for pan-macrophages CD68 antigen; (G) Ratio between M1/M2 polarized macrophages calculated on the basis of CD86/ArgI expression; (H–I) Gene expression of *Nos2* (M1) and *Arginase I* (M2) in treated diaphragms throughout the time points. *B2m* was used as housekeeping gene; (J) Ratio between *Nos2/ArgI* expression. N = native tissue, P = patch, L = liver. **p < .01; ***p < .001; n.s. = not significant by ANOVA test. Scale bar = 100 μm.

the same surgical approach described in the previous section. Histological analyses showed comparable cell invasion and matrix remodelling as highlighted in the wt mice (Fig. 5A). After patch implantation, the overall thickness of atrophic diaphragm gradually increased during the time points reaching the same thickness of the wt diaphragm (Fig. 5B). The thickness enhancement in *HSA-Cre*,

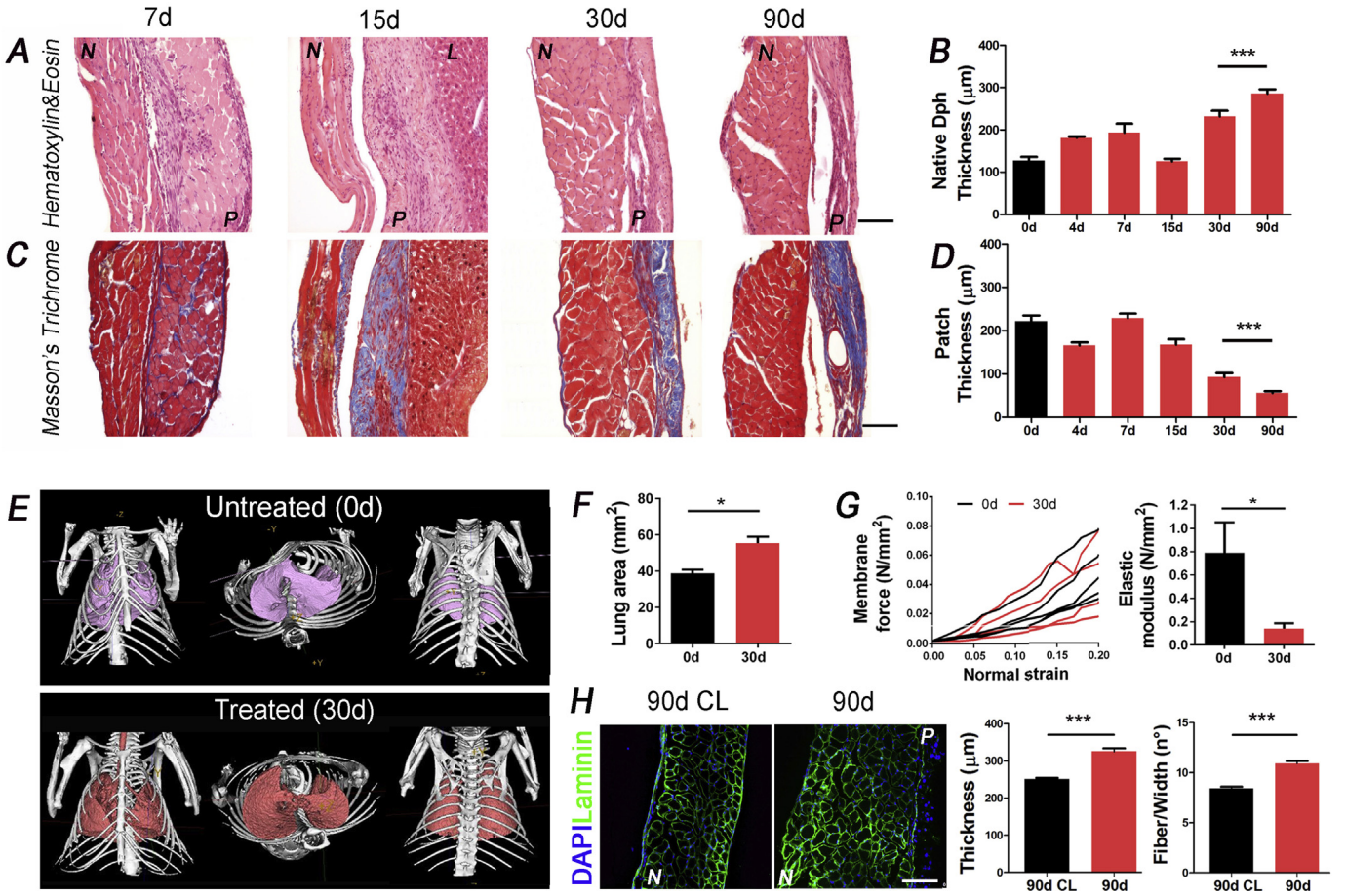

Fig. 5. Diaphragm regeneration in atrophic *HSA-Cre*, $Smn^{F7/F7}$ mouse model. (A,C) Histological appearance of treated diaphragms after 7, 15, 30 and 90 days from implantation; (B,D) Thickness of native atrophic diaphragm and implanted patch throughout all the time points; (E,F) CT scan and lung area of untreated (0d) and treated (30d) mice; (G) Mechanical properties of untreated (0d) and treated (30) atrophic diaphragm; (H) Comparison between diaphragm treated side (90d) and non-treated contralateral (CL) side (90d CL) in terms of thickness and number of fibers. N = native tissue, P = patch, L = liver. *p < .05; ***p < .001 by Student *t*-test; scale bar = 100 μm.

$Smn^{F7/F7}$ atrophic recipient was delayed in respect to the growth observed in wt recipient, but notably, a decrease to basal level did not appear in the analysed period. In parallel, the implanted patch was greatly reabsorbed with no differences when compared to kinetic to the wt implant (Fig. 5C, D). Importantly, *HSA-Cre*, $Smn^{F7/F7}$ atrophic mice with healthy acellular matrix displayed amelioration of the thoracic cage, lung morphology and area 30 days from implantation (Fig. 5E). The thoracic cage of *HSA-Cre*, $Smn^{F7/F7}$ mice showed deformation and limited pulmonary space due to the atrophic muscles of the chest. At 30 days post-implantation treated animals demonstrated a rearrangement of the thoracic space with an increased lung area. Importantly, amelioration of the thoracic space was also confirmed by mechanical tests. Although treated (30d) and untreated (0d) atrophic diaphragms possess comparable deformation ability, elastic modulus demonstrated that 30 days after patch implantation, treated muscles increased their strain resistance, acquiring elastic properties comparable to those of healthy diaphragm (Fig. 5F). Moreover, comparing treated and non-treated (CL, contralateral) side of the same atrophic diaphragm 90 days post-implantation, it was evident the thickening of native tissue in the treated area and the increasing of fibres number always in respect to its contralateral side (Fig. 5G).

Despite the tissue morphological amelioration, especially after 30 days of treatment (Fig. 6A), CSA of atrophic diaphragm fibres showed no significant differences when compare to untreated animals, similarly to wt recipients. Nevertheless, there was a difference among the time points in CSA distribution, since 4 days after treatment about 80% of fibres possessed an average area of less than 500 μm^2 (Fig. 6B). This data correlates with an up-regulation of Myh3 gene and protein expression, underling the same mechanism of new fibre generation as occurred in wt treated mice (Fig. 6C). Cell activation and proliferation was lower but prolonged when compared to wt diaphragm response, as highlighted by Ki67 staining. Proliferating cells increased significantly at 4 days and remained until 90 days post-implantation (Fig. 6D). Myogenic cell activation was evident by the enhanced number of MyoD positive cells detected in the native atrophic diaphragm at early time points (Fig. 6G) and by increased expression of genes related with muscle regeneration (Fig. 6H). The inflammatory response of the native atrophic diaphragm to the implantation of wt-derived acellular matrix was slightly different in comparison with a wt recipient. CD86 positive macrophages (M1 polarized) were already detected in the untreated atrophic diaphragm and increased after 4 and 7 days from the implantation, however *Nos2* expression trend indicated a decrease in M1 macrophage polarization during the treatment period (Fig. 6E, F). Importantly, *ArgI* was progressively activated, confirming also in this atrophic mouse model the pro-regenerative and anti-inflammation effect of the implanted acellular matrix (Fig. 6E, F).

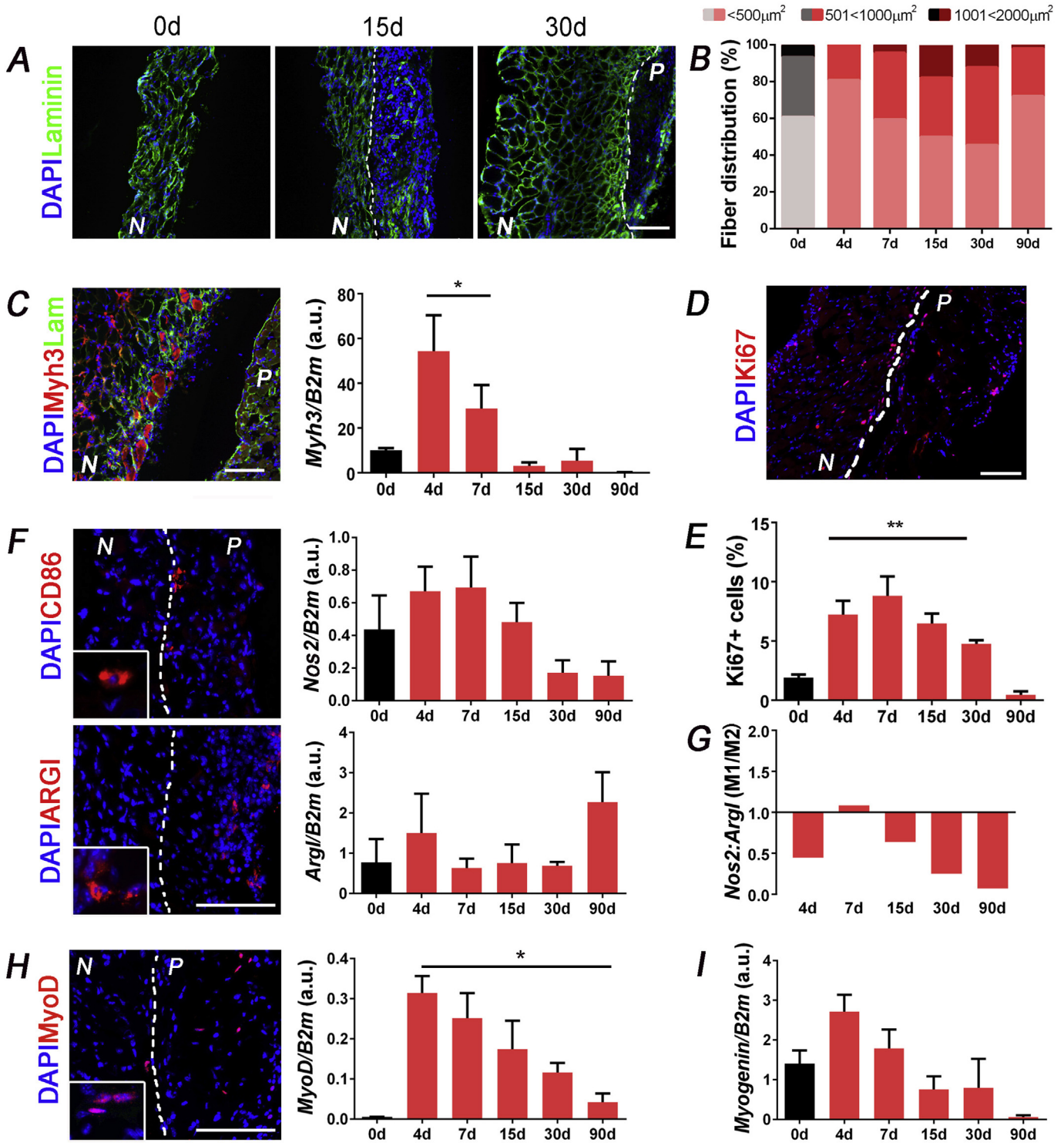

Fig. 6. Inflammatory response and myogenic cell activation in treated atrophic diaphragm. (A) Immunostaining for Laminin of treated muscles at different time points; (B) CSA fiber distribution during the time points; (C) Representative immunostaining (4 days) and quantification of *Myh3* expression at the different time points; (D,E) Representative immunostaining (7 days) and quantification of proliferating Ki67 + cells; (F) Immunostaining and RealTime PCR quantification of M1 (CD86 and *Nos2*) and M2 (Arginase I) monocyte polarization at the different time points; (G) Ratio between M1/M2 polarized macrophages calculated on the basis of *Nos2/Argl* expression; (H) Immunostaining and PCR quantification of MyoD + precursor cells in treated samples. (I) RealTime PCR quantification of *Myogenin* during the time points; *B2m* was used as housekeeping gene. N = native tissue, P = patch, L = liver. *p < .05; **p < .01 by ANOVA test; scale bar = 100 μm.

3. Discussion

In this work, we focused on the production and characterization of a biological scaffold obtained through the DET protocol, with the aim of using an ECM-derived construct as a patch to promote regeneration and repair in skeletal muscle diseases. Decellularized tissues were obtained removing the cellular fraction from fresh tissues, preserving structure and composition of the original ECM.

They represent a useful tool for the study of biochemical and biomechanical properties of the ECM and to fabricate tissue-specific scaffolds for regenerative medicine application.

The use of decellularized ECM as a patch offers the advantages of having a substrate that perfectly mimics architecture and organization of the native tissue and presents the same biochemical composition, cell homing activation, biomechanical and angiogenic properties. Using DET protocol, we were able to obtain a well preserved skeletal muscle matrix that possessed the same protein composition and distribution of a fresh tissue, but with depletion of nuclei content. Drastic decrease in DNA quantity and cell number in the treated tissue is a crucial outcome in decellularization methods and here we obtained highly significant cell depletion in order to avoid any *in vivo* immune-related rejection of the scaffold. Interestingly, histological and ultrastructural analyses demonstrated that acellular scaffolds maintained intact the myofibres, the major skeletal muscle component. Preservation of muscle fibres after decellularization allowed the matrix to have similar structure, biomechanical properties and elasticity to the fresh tissue, key features in engineering skeletal muscle tissue. Moreover, a comparable stiffness before and after decellularization maintains the potential of generating physiological stimuli once the scaffold is seeded with new cells or implanted *in vivo*. This aspect is of paramount importance, as it was demonstrated that different stiffness is able to drive multiple features of cell behaviour, including proliferation and differentiation [31]. Furthermore, altering or modifying rigidity of a tissue may cause pathological fibrosis [32] or contribute to development and spread out of cancer [33,34]. It is known that many malignancies are associated with a strong fibrotic reaction, termed 'desmoplasia', which is characterized by an accumulation of fibrillar collagen types I and III and increased degradation of type IV collagen [35]. Loss of tissue architecture, altered mechanics, increased ECM rigidity due to collagen deposition and inflammation, convey a wrong set of instructions to individual cells, leading to structural changes in tissue stem cell niche, and allowing cancer cell survival and proliferation [36].

In vivo implantation of acellular ECM gave rise to changes in the local muscle characteristics. This was a result of orchestrated events and processes that range from scaffold degradation to ECM remodelling by host cells, driven mainly by an immune modulatory effect caused by the patch, as we previously described in a discordant xenotransplantation model with implantation of decellularized muscle tissues [28]. Cascade activated by this event includes promotion of a local pro-regeneration microenvironment with activation of M2 polarized macrophages [26], attraction of vessels from the host tissue [37] and recruitment of stem and progenitor cells to the site of scaffold placement [38,39]. In this *in vivo* approach, the simple application of the patch without any damage or lesion to the recipient diaphragm induced remodelling in the native tissue. Firstly, we observed an enlargement of the native diaphragm. This effect was transient in the wt mouse model, but consistent and with an increasing-pattern across all time points in the atrophic mouse model, that finally showed comparable thickness with a wt diaphragm 90 days post-implantation. This physiological reaction was not due to a compensatory hypertrophy, as it has been demonstrated with strenuous exercise and severe overloading [40]. Rather than an increase of fibre CSA, indeed, our study evidenced that the increase in thickness was accompanied with generation of new muscle fibres (Myh3 positive), especially in the areas in contact with the implanted patch. Moreover, we found neuromuscular junctions in the remodelled patch throughout the time course, as detected with α−bungarotoxin staining (data not shown), a neuromuscular toxin that recognizes nicotinic acetylcholine receptors, indicating a complete functional fusion of the applied matrix with the recipient diaphragm. This phenomenon points out how an ECM-derived scaffold alone could be used as a tool for promoting local regeneration and generation of new functional tissue. Together with the thickening of native diaphragm, the applied patch was constantly remodelled and reabsorbed by resident cells during the time points, confirming the degradation fate that classically distinguishes biological scaffolds [41].

Cell migration to the scaffold also followed a precise pattern. Firstly, CD31 + cells and small capillaries vWf+ were found within the patch (data not shown), indicating that ECM still possessed angiogenic factors necessary to attract vessels and to allow migration and repopulation by host cells [37]. Secondly, as expected, both in wt and atrophic mouse models, cells migrating to the patch were predominantly myogenic, a process that started with the activation of resident muscle stem cells in the native diaphragm. These activated progenitor cells seemed to act with a double behaviour: (a) migration into the implanted scaffold, as highlighted by presence of Myf5 and MyoD positive cells, and (b) generation of new muscle fibres in the native diaphragm, confirmed by local expression of embryonic myosin, normally absent in healthy and mature rodent muscles [42]. Importantly, we found a distinct and exclusive temporary overexpression of Myf5 in wt and MyoD in atrophic model, both at protein and gene expression level. Nevertheless, the physiological final result (i.e. generation of new muscle fibres and local thickening of treated muscles) was comparable in the two mouse models. This finding indicates that there is a different myogenic activation pathway between healthy and atrophic muscles, supporting the data that these two transcription factors can partially compensate one another during development [43–45], maintaining at the same time distinct and specific functions [46]. Of remarkable importance, in the *HSA-Cre*, $Smn^{F7/F7}$ mouse model, the positive effect of implanted patch was visible macroscopically with amelioration of the chest anatomy and increased lung area. Furthermore, improvement in the atrophic condition was detected also measuring the elastic modulus that became similar to that of wt mice.

Certainly, the largest number of cells found in the colonized patch was composed of monocytes and CD68 + cells, especially in the early time points. Together with satellite cells, also myeloid cells represent a key player in tissue regeneration, in particular in injured muscles. Researchers are investigating whether the manipulation of the latest cell population can provide novel strategies to potentiate stem cell function in muscle regeneration [47–49]. It is known that macrophages display a broad spectrum of phenotypic diversity that can be modulated by soluble factors [50–53], or by changing cell shape and connections [54], with a binary readout improving (M2 polarized) or blocking (M1 polarized) regeneration [49]. In general, the implantation of ECM-derived scaffold is characterized by immediate mononuclear cell infiltration [55]. Interestingly, in this event there is a lack of usual cytotoxic mediators of inflammation and a consequent formation of polarized type 2 T lymphocytes [56]. Together with modulation of T response, there is a rapid shift of macrophage polarization toward M2-like phenotype [26,27], occurred both in allogenic and xenogeneic transplantation models [28]. In our *in vivo* experiments, we obtained an immediate polarization of macrophages towards pro-regenerative M2 type both in wt and atrophic mice, although in the latter there was a chronic inflammatory condition characterized by substantial presence of M1 macrophages at basal level and derived by the persistent myofibres' degeneration [57,58]. This polarization was confirmed by the expression of Arginase I in cells invading the patch and by the ratio of *Nos2* and *Arginase I* gene expression always in favour of the second. In parallel, we found an increased presence of CD4+FoxP3+ cells in treated areas, a phenotype generally associated with transplant acceptance [28,59]. Up to now, less is known about the hypothesis that the process of decellularization exposes or unmasks certain surface peptides and

molecules on the scaffold that modulate the immune response [60–63]. One reliable explanation is the ability of the scaffold to activate at the beginning in the host a foreign body reaction, rapidly shifted in a pro-regenerative mechanism due to presence of cytokines and growth factors in the decellularized matrix that stimulate (together with T helper) in a very short time, macrophages, endothelial, and muscle precursor cells. It has been already demonstrated *in vitro* that products derived from ECM degradation promote M2-like macrophage phenotype polarization [27]. Although it is not clear yet what degradation product or cytokine remains within the scaffold after decellularization, the biochemical effect of these compounds is effective enough in activating the M2 macrophage polarization *in vivo*, triggering a cascade in loop that enhances the number and the effect of anti-inflammatory cells throughout all the time points. Moreover, macrophages stimulated with ECM products have been shown to promote migration and differentiation of skeletal muscle progenitor cells [27,29]. This effect was evident in our *in vivo* model, both in wt and atrophic mice, where M2 macrophage polarization and Myf5/MyoD positive cells were consequently activated.

The amelioration of a genetically impaired muscle, although only local and likely transient, after a simple implantation of a healthy muscle-derived natural matrix, is a new pivotal outcome in understanding the potential of using ECM-derived scaffolds in tissue engineering. This effect was naturally achieved in wt mice, resulting in diaphragm local thickening when in contact with the ECM-derived matrix. In the diseased *HSA-Cre*, $Smn^{F7/F7}$ mouse model the immunomodulatory-guided effect was also confirmed. It is worth of notice that despite starting from an impaired muscle characterized by chronic inflammation and dysfunctional muscle homeostasis, the pro-regenerative effect activated by the healthy ECM-derived scaffold produced a strong improvement in the anatomy of the chest and physiology of the diaphragm with elastic performances comparable with healthy muscles. This approach gives new inside about using natural-derived scaffolds developed from tissue-specific ECM and confers high potential to future projects that include seeding of precursor cells into the scaffold prior implantation. Indeed, it is possible that future therapies may combine the transplantation of healthy cells with the delivery of a "healthy" matrix.

In conclusion, this work shows the development and characterization of a tissue-specific ECM-derived scaffold that displays fundamental features for tissue regenerative and repair applications. We have shown that ECM provides anti-inflammation, pro-regenerative and cell homing properties in both healthy and diseased muscles. Besides their use for tissue engineering, we postulate that natural scaffolds are also promising candidate for the treatment of muscle diseases. This approach includes the use of acellular scaffolds also for *in vitro* studies to analyse cell engraftment, proliferation, migration and differentiation using seeding techniques for re-cellularisation purposes, in order to reproduce a viable functional muscle in culture. Further work will be essential to understand the role of all components of the ECM in its biological effect *in vivo* and how these characteristics affect cell behaviour *in vitro* and *in vivo*. Cell delivery together with the matrix may further improve affected diaphragms, potentially becoming the optimal approach for future clinical applications.

4. Methods

4.1. Animals

All surgical procedures and animal husbandry were carried out in accordance with University of Padua's Animal care and Use Committee (CEASA, protocol number 67/2011 approved on 21st September 2011) and were communicated to the Ministry of Health and local authorities in accordance with the Italian Law on the use of experimental animals (DL n. 16/92 art. 5). The following animals were used: 8–12 week-old male and female C57BL/6J mice (wt mice) as donors (diaphragms for scaffolds generation) and as recipients; *HSA-Cre*,$Smn^{F7/F7}$ as the host atrophic model.

4.2. Diaphragm decellularization

Diaphragm muscle obtained from wt mice was washed in sterile phosphate buffered saline 1X (PBS) and conserved in PBS containing 1% penicillin-streptomycin solution (PBS–P/S). Diaphragms destined to decellularization process were treated with one to four DET cycles. Each DET cycle was composed of deionized water at 4 °C for 24 h, 4% sodium deoxycholate (Sigma) at room temperature (RT) for 4 h, and 2000 kU DNase-I (Sigma) in 1 M NaCl (Sigma) at RT for 3 h, after washing in water. After decellularization, matrices were washed for at least 3 days in deionized sterile water and preserved at 4 °C in PBS-P/S or immediately analysed.

4.3. DNA isolation and quantification

To assess total DNA content within the native diaphragm and decellularized matrices, specimens were treated using DNeasy Blood&Tissue kit (Qiagen) under manufacturer's instruction. DNA samples were then quantified using Nanodrop 2000 spectrophotometer (Thermo Scientific, USA).

4.4. Immunohistochemistry and immunofluorescence

Frozen section (8–10 μm thick) were stained with H-E kit for rapid frozen section, Masson's Trichrome with aniline blue kit, Alcian blue pH 2.5 kit and WEIGERT - VAN GIESON for elastic fibres and connectivum (long method) (all from Bio-Optica, UK) under manufacturer's instruction. For immunofluorescence analysis, sections were permealised with 0.5% Triton X-100, blocked with 10% HS and incubated with primary antibodies, then slides were washed and incubated with labelled secondary Alexa Fluor secondary antibodies as listed in Supplementary Table 1. Finally, nuclei were counterstained with fluorescent mounting medium plus 100 ng/ml 4′,6-diamidino-2-phenylindole (DAPI) (Sigma–Aldrich). For each diaphragm, random pictures were collected with a direct microscope.

4.5. ECM component quantification

Collagen, sulfated glycosaminoglycan (GAGs) and elastin content on fresh and decellularized diaphragms were quantified using respectively the SIRCOL collagen assay, Blyscan GAG Assay Kit and Fastin Elastin Assay Kit (all from Biocolor, UK) under manufacturer's instruction.

4.6. Scanning electron microscopy

Samples were fixed in 2% glutaraldehyde in 0.1 M phosphate; following washing they were cut into segments of approximately 1 cm length and cryoprotected in 25% sucrose, 10% glycerol in 0.05 M PBS (pH 7.4) for 2 h, then fast frozen. The samples were then placed back into the cryoprotectant at RT and allowed to thaw. After washing, the material was fixed in 1% OsO4/0.1 M phosphate buffer (pH 7.3) and washed again. After rinsing with deionized water, specimens were dehydrated in a graded ethanol-water series to 100% ethanol, critical point dried using CO2 and finally mounted on aluminium stubs using sticky carbon taps. Samples were mounted and coated with a thin layer of Au/Pd (approximately 2 nm thick)

using a Gatan ion beam coater. Images were recorded with a Jeol 7401 FEG scanning electron microscope.

4.7. Mechanical test

The specimens were subjected to uniaxial tension until failure. This test records the displacement applied to the specimen versus corresponding value of tensile force. The nominal strain was obtained by normalizing the displacement with the initial gauge length of the specimen; the nominal stress as force for unit of initial transverse section. The response of the tissue was evaluated in terms of membrane force and Young's modulus. The membrane force is the force per unit width of the specimen. The ratio of nominal stress to nominal strain up to 5% was considered as the Young's modulus. Mechanical tests were performed in the Planar Biaxial TestBench Test Instrument Bose® Electro-Force (USA) at RT (20 ± 1 °C). Specimens in the form of strips with average width of 4 mm and 5 mm gauge length were elongated at a constant strain rate of 0.1 s^{-1}. The thickness of the samples was measured from the histologic analysis and the width by using digital images analysis. Four or five samples were considered for each evaluated tissue.

4.8. In vivo implantation

Wt and *HSA-Cre,Smn*$^{F7/F7}$ mice were gently handled in general anaesthesia with O_2 and isofluorane (Forane, Merial, IT) (3–3.5% for induction and, subsequently, 2% for maintenance) inhalation via facemask, potentiated with the analgesic tramadol. After a 3 cm long median superior incision, the diaphragm was visualized. A decellularized patch of about 5 × 3 mm was placed onto the native diaphragm, and fixed with three or four stitches of Prolene 9/0. Organs were then repositioned into the abdominal cavity, the abdominal wall was closed in two layers and the animals left to wake up under a heating lamp. Afterwards, the animals were checked to ensure arousal within 10 min after surgery and moved back to their cages monitored for activity, ability to drink and eat and for signs of bleeding or infection. Analgesics (as painkillers), antibiotics and saline solution (for rehydratation) were administered. Mice were euthanized by cervical dislocation at 4, 7, 15, 30 and 90 days post implantation.

4.9. MicroCt scan

Prior to imaging, mice were anesthetized (with a mixture of Rompum and Zoletil given i.p.), and imaged on the eXplore Locus SP (GE Healthcare). Image processing and data analysis were performed using eXplore MicroView software 2.0 (GE Healthcare).

4.10. Real time PCR

Total RNA has been extracted using RNeasy Plus Mini kit (QIAGEN GmbH) following the supplier's instructions. RNA has been quantified with a ND-2000 spectrophotometer and 1 μg has been retrotranscripted with SuperScript II and related products (all from Life Technologies) in a 20 μl reaction. Real-time PCR reactions were performed using a LightCycler II (Roche, Monza, Italy). Reactions have been carried out in triplicate using 4 μl of FASTSTART SYBR GREEN MASTER (Roche) and 2 μl of primers mix FW + REV (final concentration, 300/300 nM) in a final volume of 20 μl. Serial dilutions of a positive control sample have been used to create a standard curve for the relative quantification. The amount of each mRNA has been normalized for the content in β2-microglobulin. Primer sequences are listed in Supplementary Table 2.

4.11. Statistical analysis

Data are expressed as means ± SEM, or as means ± SD. For immunofluorescence and immunohistochemical analyses, at least 15 random high-power field areas were considered per each analysed muscle. Statistical significance was determined using an equal-variance Student's t test, two-way analysis of variance (ANOVA) test, and the Mann–Whitney U test (for quantitative real time-polymerase chain reaction [qRT-PCR] analyses). A p value below 0.05 was considered to be statistically significant.

Author contributions

Ma.Pi. and L.U. designed and performed the experiments, analysed the data and wrote the manuscript; M.E.A.-F., C.F. and B.E. performed experiments and analysed the data; A.D. performed surgical procedures; G.Z. and A.R. performed scan imaging; P.P. and N.E. performed mechanical tests; P.D.C. and Mi.Po. supervised the project discussed the data and wrote the manuscript.

Competing interests

All the authors declare no conflict of interest.

Acknowledgements and funding

Supported by research grant CARIPARO-IRP Ricerca Pediatrica (Grant number 13/04) 2012/2014 “A tissue engineering approach for diaphragm repair in a congenital diaphragmatic hernia mouse model”; University of Padova, Progetto di Ateneo 2012/2014 “Decellularized matrix for diaphragm repair through a tissue engineering approach”. Ma.Pi., C.F. and Mi.Po. are supported by Istituto di Ricerca Pediatrica Città della Speranza (Grant number 12/01); L.U. and P.D.C are supported by GOSH and NIHR (RP-2014-04-046).

Appendix A. Supplementary data

Supplementary data related to this article can be found at http://dx.doi.org/10.1016/j.biomaterials.2015.10.005.

References

[1] P. Atluri, A. Trubelja, A.S. Fairman, P. Hsiao, J.W. MacArthur, J.E. Cohen, et al., Normalization of postinfarct biomechanics using a novel tissue-engineered angiogenic construct, Circulation 128 (2013) S95–S104.
[2] S.F. Badylak, P.V. Kochupura, I.S. Cohen, S.V. Doronin, A.E. Saltman, T.W. Gilbert, et al., The use of extracellular matrix as an inductive scaffold for the partial replacement of functional myocardium, Cell Transplant. 15 (Suppl. 1) (2006) S29–S40.
[3] P.V. Kochupura, E.U. Azeloglu, D.J. Kelly, S.V. Doronin, S.F. Badylak, I.B. Krukenkamp, et al., Tissue-engineered myocardial patch derived from extracellular matrix provides regional mechanical function, Circulation 112 (2005) I144–I149.
[4] R.N. Chen, H.O. Ho, Y.T. Tsai, M.T. Sheu, Process development of an acellular dermal matrix (ADM) for biomedical applications, Biomaterials 25 (2004) 2679–2686.
[5] H. Koch, C. Graneist, F. Emmrich, H. Till, R. Metzger, H. Aupperle, et al., Xenogenic esophagus scaffolds fixed with several agents: comparative in vivo study of rejection and inflammation, J. Biomed. Biotechnol. 2012 (2012) 948320.
[6] S. Sjoqvist, P. Jungebluth, M.L. Lim, J.C. Haag, Y. Gustafsson, G. Lemon, et al., Experimental orthotopic transplantation of a tissue-engineered oesophagus in rats, Nat. Commun. 5 (2014) 3562.
[7] M.J. Elliott, P. De Coppi, S. Speggiorin, D. Roebuck, C.R. Butler, E. Samuel, et al., Stem-cell-based, tissue engineered tracheal replacement in a child: a 2-year follow-up study, Lancet 380 (2012) 994–1000.
[8] P. Macchiarini, P. Jungebluth, T. Go, M.A. Asnaghi, L.E. Rees, T.A. Cogan, et al., Clinical transplantation of a tissue-engineered airway, Lancet 372 (2008) 2023–2030.
[9] B.M. Sicari, J.P. Rubin, C.L. Dearth, M.T. Wolf, F. Ambrosio, M. Boninger, et al.,

An acellular biologic scaffold promotes skeletal muscle formation in mice and humans with volumetric muscle loss, Sci. Transl. Med. 6 (2014) 234–258.
[10] M.T. Conconi, P. De Coppi, S. Bellini, G. Zara, M. Sabatti, M. Marzaro, et al., Homologous muscle acellular matrix seeded with autologous myoblasts as a tissue-engineering approach to abdominal wall-defect repair, Biomaterials 26 (2005) 2567–2574.
[11] M.J. Cozad, S.L. Bachman, S.A. Grant, Assessment of decellularized porcine diaphragm conjugated with gold nanomaterials as a tissue scaffold for wound healing, J. Biomed. Mater. Res. Part A 99 (2011) 426–434.
[12] C.R. Deeken, M. Esebua, S.L. Bachman, B.J. Ramshaw, S.A. Grant, Assessment of the biocompatibility of two novel, bionanocomposite scaffolds in a rodent model, J. Biomed. Mater. Res. Part B Appl. Biomater. 96 (2011) 351–359.
[13] M.A. Machingal, B.T. Corona, T.J. Walters, V. Kesireddy, C.N. Koval, A. Dannahower, et al., A tissue-engineered muscle repair construct for functional restoration of an irrecoverable muscle injury in a murine model, Tissue Eng. Part A 17 (2011) 2291–2303.
[14] B. Perniconi, A. Costa, P. Aulino, L. Teodori, S. Adamo, D. Coletti, The pro-myogenic environment provided by whole organ scale acellular scaffolds from skeletal muscle, Biomaterials 32 (2011) 7870–7882.
[15] C.A. Rossi, M. Flaibani, B. Blaauw, M. Pozzobon, E. Figallo, C. Reggiani, et al., In vivo tissue engineering of functional skeletal muscle by freshly isolated satellite cells embedded in a photopolymerizable hydrogel, FASEB J Off. Publ. Fed. Am. Soc. Exp. Biol. 25 (2011) 2296–2304.
[16] L. Wang, J.A. Johnson, D.W. Chang, Q. Zhang, Decellularized musculofascial extracellular matrix for tissue engineering, Biomaterials 34 (2013) 2641–2654.
[17] M.T. Wolf, K.A. Daly, J.E. Reing, S.F. Badylak, Biologic scaffold composed of skeletal muscle extracellular matrix, Biomaterials 33 (2012) 2916–2925.
[18] D. Skuk, B. Roy, M. Goulet, P. Chapdelaine, J.P. Bouchard, R. Roy, et al., Dystrophin expression in myofibers of Duchenne muscular dystrophy patients following intramuscular injections of normal myogenic cells, Mol. Ther. J. Am. Soc. Gene Ther. 9 (2004) 475–482.
[19] C. Alexakis, T. Partridge, G. Bou-Gharios, Implication of the satellite cell in dystrophic muscle fibrosis: a self-perpetuating mechanism of collagen over-production, Am. J. Physiol. Cell Physiol. 293 (2007) C661–C669.
[20] L.K. Wood, E. Kayupov, J.P. Gumucio, C.L. Mendias, D.R. Claflin, S.V. Brooks, Intrinsic stiffness of extracellular matrix increases with age in skeletal muscles of mice, J. Appl. Physiol. 117 (2014) 363–369.
[21] J.J. Song, H.C. Ott, Organ engineering based on decellularized matrix scaffolds, Trends Mol. Med. 17 (2011) 424–432.
[22] S. Crawley, E.M. Farrell, W. Wang, M. Gu, H.Y. Huang, V. Huynh, et al., The alpha7beta1 integrin mediates adhesion and migration of skeletal myoblasts on laminin, Exp. Cell Res. 235 (1997) 274–286.
[23] R. Flaumenhaft, D. Moscatelli, O. Saksela, D.B. Rifkin, Role of extracellular matrix in the action of basic fibroblast growth factor: matrix as a source of growth factor for long-term stimulation of plasminogen activator production and DNA synthesis, J. Cell. Physiol. 140 (1989) 75–81.
[24] L. Arnold, A. Henry, F. Poron, Y. Baba-Amer, N. van Rooijen, A. Plonquet, et al., Inflammatory monocytes recruited after skeletal muscle injury switch into antiinflammatory macrophages to support myogenesis, J. Exp. Med. 204 (2007) 1057–1069.
[25] S.C. Bryer, G. Fantuzzi, N. Van Rooijen, T.J. Koh, Urokinase-type plasminogen activator plays essential roles in macrophage chemotaxis and skeletal muscle regeneration, J. Immunol. 180 (2008) 1179–1188.
[26] B.N. Brown, J.E. Valentin, A.M. Stewart-Akers, G.P. McCabe, S.F. Badylak, Macrophage phenotype and remodeling outcomes in response to biologic scaffolds with and without a cellular component, Biomaterials 30 (2009) 1482–1491.
[27] B.M. Sicari, J.L. Dziki, B.F. Siu, C.J. Medberry, C.L. Dearth, S.F. Badylak, The promotion of a constructive macrophage phenotype by solubilized extracellular matrix, Biomaterials 35 (2014) 8605–8612.
[28] J.M. Fishman, M.W. Lowdell, L. Urbani, T. Ansari, A.J. Burns, M. Turmaine, et al., Immunomodulatory effect of a decellularized skeletal muscle scaffold in a discordant xenotransplantation model, Proc. Natl. Acad. Sci. U. S. A. 110 (2013) 14360–14365.
[29] M.M. Stern, R.L. Myers, N. Hammam, K.A. Stern, D. Eberli, S.B. Kritchevsky, et al., The influence of extracellular matrix derived from skeletal muscle tissue on the proliferation and differentiation of myogenic progenitor cells ex vivo, Biomaterials 30 (2009) 2393–2399.
[30] K.M. Brouwer, W.F. Daamen, D. Reijnen, R.H. Verstegen, G. Lammers, T.G. Hafmans, et al., Repair of surgically created diaphragmatic defect in rat with use of a crosslinked porous collagen scaffold, J. Tissue Eng. Regen. Med. 7 (2013) 552–561.
[31] S. Dupont, L. Morsut, M. Aragona, E. Enzo, S. Giulitti, M. Cordenonsi, et al., Role of YAP/TAZ in mechanotransduction, Nature 474 (2011) 179–183.
[32] P.A. Janmey, R.G. Wells, R.K. Assoian, C.A. McCulloch, From tissue mechanics to transcription factors, Differ. Res. Biol. Divers. 86 (2013) 112–120.
[33] I. Levental, K.R. Levental, E.A. Klein, R. Assoian, R.T. Miller, R.G. Wells, et al., A simple indentation device for measuring micrometer-scale tissue stiffness, J. Phys. Condens. Matter Inst. Phys. J 22 (2010) 194120.
[34] J. Schrader, T.T. Gordon-Walker, R.L. Aucott, M. van Deemter, A. Quaas, S. Walsh, et al., Matrix stiffness modulates proliferation, chemotherapeutic response, and dormancy in hepatocellular carcinoma cells, Hepatology 53 (2011) 1192–1205.
[35] M. Egeblad, M.G. Rasch, V.M. Weaver, Dynamic interplay between the collagen scaffold and tumor evolution, Curr. Opin. Cell Biol. 22 (2010) 697–706.
[36] S. Piccolo, S. Dupont, M. Cordenonsi, The biology of YAP/TAZ: hippo signaling and beyond, Physiol. Rev. 94 (2014) 1287–1312.
[37] J.E. Valentin, J.S. Badylak, G.P. McCabe, S.F. Badylak, Extracellular matrix bioscaffolds for orthopaedic applications. A comparative histologic study, J. Bone Jt. Surg. Am. 88 (2006) 2673–2686.
[38] A.J. Beattie, T.W. Gilbert, J.P. Guyot, A.J. Yates, S.F. Badylak, Chemoattraction of progenitor cells by remodeling extracellular matrix scaffolds, Tissue Eng. Part A 15 (2009) 1119–1125.
[39] J.E. Reing, L. Zhang, J. Myers-Irvin, K.E. Cordero, D.O. Freytes, E. Heber-Katz, et al., Degradation products of extracellular matrix affect cell migration and proliferation, Tissue Eng. Part A 15 (2009) 605–614.
[40] G.R. Adams, M.M. Bamman, Characterization and regulation of mechanical loading-induced compensatory muscle hypertrophy, Compr. Physiol. 2 (2012) 2829–2870.
[41] T.W. Gilbert, A.M. Stewart-Akers, S.F. Badylak, A quantitative method for evaluating the degradation of biologic scaffold materials, Biomaterials 28 (2007) 147–150.
[42] S. Schiaffino, L. Gorza, G. Pitton, L. Saggin, S. Ausoni, S. Sartore, et al., Embryonic and neonatal myosin heavy chain in denervated and paralyzed rat skeletal muscle, Dev. Biol. 127 (1988) 1–11.
[43] T. Braun, M.A. Rudnicki, H.H. Arnold, R. Jaenisch, Targeted inactivation of the muscle regulatory gene Myf-5 results in abnormal rib development and perinatal death, Cell 71 (1992) 369–382.
[44] M.A. Rudnicki, T. Braun, S. Hinuma, R. Jaenisch, Inactivation of MyoD in mice leads to up-regulation of the myogenic HLH gene Myf-5 and results in apparently normal muscle development, Cell 71 (1992) 383–390.
[45] Z. Yablonka-Reuveni, M.A. Rudnicki, A.J. Rivera, M. Primig, J.E. Anderson, P. Natanson, The transition from proliferation to differentiation is delayed in satellite cells from mice lacking MyoD, Dev. Biol. 210 (1999) 440–455.
[46] K. Day, B. Paterson, Z. Yablonka-Reuveni, A distinct profile of myogenic regulatory factor detection within Pax7+ cells at S phase supports a unique role of Myf5 during posthatch chicken myogenesis, Dev. Dyn. Off Publ. Am. Assoc. Anat. 238 (2009) 1001–1009.
[47] M.L. Novak, E.M. Weinheimer-Haus, T.J. Koh, Macrophage activation and skeletal muscle healing following traumatic injury, J. Pathol. 232 (2014) 344–355.
[48] M. Saclier, H. Yacoub-Youssef, A.L. Mackey, L. Arnold, H. Ardjoune, M. Magnan, et al., Differentially activated macrophages orchestrate myogenic precursor cell fate during human skeletal muscle regeneration, Stem Cells 31 (2013) 384–396.
[49] J.G. Tidball, K. Dorshkind, M. Wehling-Henricks, Shared signaling systems in myeloid cell-mediated muscle regeneration, Development 141 (2014) 1184–1196.
[50] C.D. Mills, K. Kincaid, J.M. Alt, M.J. Heilman, A.M. Hill, M-1/M-2 macrophages and the Th1/Th2 paradigm, J. Immunol. 164 (2000) 6166–6173.
[51] J.L. Pace, S.W. Russell, B.A. Torres, H.M. Johnson, P.W. Gray, Recombinant mouse gamma interferon induces the priming step in macrophage activation for tumor cell killing, J. Immunol. 130 (1983) 2011–2013.
[52] R. Philip, L.B. Epstein, Tumour necrosis factor as immunomodulator and mediator of monocyte cytotoxicity induced by itself, gamma-interferon and interleukin-1, Nature 323 (1986) 86–89.
[53] M. Stein, S. Keshav, N. Harris, S. Gordon, Interleukin 4 potently enhances murine macrophage mannose receptor activity: a marker of alternative immunologic macrophage activation, J. Exp. Med. 176 (1992) 287–292.
[54] F.Y. McWhorter, T. Wang, P. Nguyen, T. Chung, W.F. Liu, Modulation of macrophage phenotype by cell shape, Proc. Natl. Acad. Sci. U. S. A. 110 (2013) 17253–17258.
[55] S. Badylak, K. Kokini, B. Tullius, A. Simmons-Byrd, R. Morff, Morphologic study of small intestinal submucosa as a body wall repair device, J. Surg. Res. 103 (2002) 190–202.
[56] A.J. Allman, T.B. McPherson, S.F. Badylak, L.C. Merrill, B. Kallakury, C. Sheehan, et al., Xenogeneic extracellular matrix grafts elicit a TH2-restricted immune response, Transplantation 71 (2001) 1631–1640.
[57] S. Nicole, B. Desforges, G. Millet, J. Lesbordes, C. Cifuentes-Diaz, D. Vertes, et al., Intact satellite cells lead to remarkable protection against Smn gene defect in differentiated skeletal muscle, J. Cell Biol. 161 (2003) 571–582.
[58] M. Piccoli, C. Franzin, E. Bertin, L. Urbani, B. Blaauw, A. Repele, et al., Amniotic fluid stem cells restore the muscle cell niche in a HSA-Cre, Smn(F7/F7) mouse model, Stem Cells 30 (2012) 1675–1684.
[59] A.J. Allman, T.B. McPherson, L.C. Merrill, S.F. Badylak, D.W. Metzger, The Th2-restricted immune response to xenogeneic small intestinal submucosa does not influence systemic protective immunity to viral and bacterial pathogens, Tissue Eng. 8 (2002) 53–62.
[60] P.L. Bollyky, B.A. Falk, R.P. Wu, J.H. Buckner, T.N. Wight, G.T. Nepom, Intact extracellular matrix and the maintenance of immune tolerance: high molecular weight hyaluronan promotes persistence of induced CD4+CD25+ regulatory T cells, J. Leukoc. Biol. 86 (2009) 567–572.
[61] P.L. Bollyky, R.P. Wu, B.A. Falk, J.D. Lord, S.A. Long, A. Preisinger, et al., ECM components guide IL-10 producing regulatory T-cell (TR1) induction from effector memory T-cell precursors, in: Proceedings of the National Academy of Sciences of the United States of America vol. 108, 2011, pp. 7938–7943.
[62] S.R. Morwood, L.B. Nicholson, Modulation of the immune response by extracellular matrix proteins, Arch. Immunol. Ther. Exp. 54 (2006) 367–374.
[63] A.H. Thomas, E.R. Edelman, C.M. Stultz, Collagen fragments modulate innate immunity, Exp. Biol. Med. 232 (2007) 406–411.